

Article

Strength Behavior and Ultimate Capacity Prediction of Self-Compacting Concrete-Filled Thin-Walled Medium-Length Steel Tubular Columns under Eccentric Compression

Yunyang Wang ^{1,*} , Shengwei Sun ², Liqing Zhang ^{3,*} and Yandong Jia ⁴¹ School of Civil and Architecture Engineering, Hunan University of Arts and Science, Changde 415000, China² China Construction Second Engineering Bureau Co., Ltd., Beijing 100054, China³ School of Civil Engineering and Architecture, East China Jiaotong University, Nanchang 330013, China⁴ School of Civil and Architecture Engineering, Liaoning University of Technology, Jinzhou 121000, China

* Correspondence: hnwangyunyang@126.com (Y.W.); zlq@ecjtu.edu.cn (L.Z.); Tel.: +86-15211204091 (Y.W.)

Abstract: The development of self-compacting concrete-filled thin-walled steel tubular columns is a potential strategy to ease the challenge of conserving resources in society, which are largely consumed by the quickly developing civil industry. However, the application of these columns in the civil industry is rare due to insufficient research, especially research concerning the strength behaviors of the columns under eccentric compression. Therefore, the eccentric compressive behaviors of medium-length tubular columns made up of self-compacting concrete and thin-walled steel with circular sections were experimentally studied in the present paper. The feasibility of predicting the columns' ultimate capacities using existing design codes was explored, and then comparisons between the predictions and experimental values were carried out. The results showed that the eccentric compression columns had a failure morphology, buckling together with a lateral deflection while they were moved from the bottom to middle positions as the wall thickness increased. Moreover, the ratios of the predicted ultimate capacity of the eccentric compressive columns to the experimental values were within the range of 0.35 to 0.94. This indicates that the predicted ultimate capacity is conservative and safe. The codes AISC-LRFD and JCJ 01-89 achieved the most conservative and the most precise predictive results, respectively. Additionally, the decrease ratio of the predicted ultimate capacity of the eccentric compressive columns to the experimental values was more evident than that of axial compressive columns. This paper can serve as guidance for the design and application of these columns, as well as foster a sustainable and resilient civil industry.

Keywords: strength behavior; thin-walled steel tubular; eccentric compression; medium-length columns; ultimate capacity prediction



Citation: Wang, Y.; Sun, S.; Zhang, L.; Jia, Y. Strength Behavior and Ultimate Capacity Prediction of Self-Compacting Concrete-Filled Thin-Walled Medium-Length Steel Tubular Columns under Eccentric Compression. *Buildings* **2023**, *13*, 2876. <https://doi.org/10.3390/buildings13112876>

Academic Editor: Ramadhansyah Putra Jaya

Received: 12 October 2023

Revised: 5 November 2023

Accepted: 7 November 2023

Published: 16 November 2023



Copyright: © 2023 by the authors. Licensee MDPI, Basel, Switzerland. This article is an open access article distributed under the terms and conditions of the Creative Commons Attribution (CC BY) license (<https://creativecommons.org/licenses/by/4.0/>).

1. Introduction

Concrete-filled steel tubes (CFSTs) have the advantage of high lateral stiffness, high strength, and excellent efficiency during the construction process; further, they are economical, which is attractive for applications in civil infrastructures, including large-span bridges [1,2], offshore structures [3,4], high-rise buildings [5], and tunnels [6,7]. The steel tubes can restrain the concrete, thus enhancing its strength and ductility. Meanwhile, the concrete can prevent the steel tubes from inward buckling [8]. Thus, the excellent composite effect of both concrete and steel tubes can enhance the behaviors of CFSTs. In addition, construction efficiency can be increased, and costs can be saved, because the steel tubes can work as molds during the process of casting the concrete [9].

The key parameters in previous research on CFST columns include the ratios of D/t and L/D , cross-section types, slenderness, material properties, bonding effect between steel tubes and concrete, and loading types [10–12]. The columns have a higher ultimate capacity when L/D and D/t are less than 11.0 and 60.0, respectively [13], as well as when

L/D and D/t are less than 15.0 and 90.0, respectively [14]. This is because the concrete inside the columns is under triaxial compression due to its confinement by the steel tube; thus, its strength is improved. Moreover, a smaller D/t ratio can increase the yield strength and improve the post-yield behaviors of the columns [15]. Nevertheless, the concrete can be restrained well with circular and octagonal sections of steel tubes, while a smaller confinement is provided by square sections, which only exists at corner regions. This is because of the different mechanisms between the different cross sections and concrete. The pressure on the concrete is generated by the plate-bending effect of the steel tube with square cross sections, while the pressure on the concrete originates from the circular stress of the steel tubes with circular cross sections [16]. At the same time, the failure of the short columns is characterized by concrete crushing and local buckling, which is caused by the steel tubes. Nevertheless, the medium-length columns exhibit partial yielding of the steel tubes and cracking of the concrete at the failure stage. Moreover, the columns with greater slenderness present overall buckling at the failure stage [17].

Hu et al. compared the restraining effect caused by square and circular sections of CFST columns. They demonstrated that the circular columns with a D/t ratio lower than 40 had a remarkable restraining effect, while the square section had no restraining effect [17]. Gupta et al. considered the D/t ratios of circular columns within the range of 25 to 39 and evaluated their properties. They pointed out that steel tubes can offer excellent confinement with lower D/t ratios [11]. Zhu et al. reported that local buckling tends to be generated at the middle location and the ends when columns are more slender [18]. Zhou et al. stated that high-strength concrete can improve the ultimate capacity of columns. Nevertheless, uneven failure and sudden crushing is not prevented [19]. Liao et al. indicated that the confinement exerted on the concrete in columns with circular sections is improved by increasing the steel content [20]. Xu et al. reported that the ductility of columns with circular sections decreases with an increase in the concrete strength [21].

Replacing normal steel tubes with thin-walled steel tubes for CFST column applications can reduce costs. Moreover, this will also ease the strain on resources, which are largely consumed by the quickly developing civil industry. Thus, given the rapid development of high-strength steel, thin-walled steel tubes can begin to be applied to CFST columns. However, the stability and maximum load of the concrete-filled thin-walled steel tubular columns are reduced [22,23]. The ductility of the columns is also reduced with increasing D/t ratios [24]. Liang et al. have predicted the maximum load and local buckling of the columns using the nonlinear fiber element method [25]. The hysteretic behaviors, including the ductility, stiffness, and energy dissipation of the columns, have been analyzed using the quasi-static cyclic loading method [26–28].

Recently, researchers have focused on self-compacting concrete-filled thin-walled steel tubes (SCFTSTs) for their outstanding advantages [29–31]. Self-compacting concrete presents good segregation resistance and high deformability. It can spread complicated molds efficiently and does not need external vibration, thus providing a high passing and filling ability. Moreover, construction time and labor costs will be saved [32–34]. If the wall thickness is lower than 3.0 mm or the confinement coefficient is less than 0.5, the steel tube is considered a thin-walled steel tube [35], which can decrease steel consumption, thus saving costs [36,37]. The mechanical behaviors of SCFTST columns under eccentric loads have been investigated by Yu et al. They measured the mechanical performance and pointed out that when the eccentric distance increases, ductility increases, while the ultimate capacity decreases [38]. Wang et al. investigated the influence of D/t ratios on failure morphology and deformation characteristics, as well as the maximum load of the axial-loaded columns. They reported that the columns present buckling at the failure stage, and the values decrease while the ultimate capacity increases when the wall thickness increases [39]. Chen and Jin researched the axial performance of columns with square, rectangular, and X sections. They examined the variation rules of strain/displacement and load, and stated that the expansion in the local position can be enhanced by intermediate stiffeners of columns with X sections. They also reported that the ultimate capacity predicted by the AISC

code is conservative [40]. Jiang et al. investigated the SCFTST elements with square and rectangular sections undergoing a bending load. They determined the failure morphology, variation in the load with displacement, and ultimate capacity. A prediction model of the mechanical performance of the elements under a bending load was proposed [41].

The ultimate capacity of CFST columns can be predicted with both formulas proposed by researchers and design codes, which is important for design. The predicted ultimate capacity using code AISC360-10 is conservative [42–44]. However, the predicted results using code EC4 are precise [10]. The peak load of normal CFST columns can be well predicted by design codes [45]. However, codes are not recommended prediction formulas for the peak load of the SCFTST members.

As the analysis of previous research shows, recent studies have mainly concentrated on the axial compression behaviors of normal steel tubular columns filled with concrete. However, research on predicting the ultimate capacity of thin-walled steel tubular columns filled with self-compacting concrete undergoing eccentric compression is rarely conducted. These types of columns are potential candidates for structure members, and are mostly applied in complex force states. Thus, the feasibility of using existing specifications to predict the bearing capacity and their service behavior analysis is important and challenging work to be explored. The present paper firstly explores the eccentric compressive behaviors of thin-walled steel tubular columns filled with self-compacting concrete. Then, the prediction of the ultimate capacity using different design codes when the columns are under eccentric compression is discussed. Additionally, the predicted ultimate capacity is compared with the experimental values. The feasibility of predicting the ultimate capacity of eccentric compressive columns is also discussed in depth. This paper can serve as guidance in the future design and application of the studied columns which can substantially improve the civil industry.

2. Experiments

2.1. Sample Fabrication

The circular columns were divided into two groups corresponding to wall thicknesses of 1.2 and 3.0 mm. Eccentric compression was applied to one group of specimens, and axial compression to the other as the control. The main parameters were the eccentricity ratio and wall thickness. Two eccentricity ratios of 0 and 0.29 were considered. Parameters of the columns are listed in Table 1; their values were determined according to [21] together with the experimental results. D , t , and L stand for the diameter, wall thickness, and height of the samples, respectively. A and E refer to axial and eccentric compression, respectively. N stands for the self-compacting concrete, and its mix design is listed in Table 2, which was determined by the experiments and the design code [46]. $T1$ and $T2$ represent wall thicknesses of 1.2 and 3.0 mm, respectively. e and r are the eccentricity of loading and the column's outer radius, respectively.

Table 1. Parameters of the SCFTST columns.

Numbers	$D \times t \times L$ (mm^3)	e (mm)	e/r
A-N-T1	$140 \times 1.2 \times 700$	0	0
E-N-T1	$140 \times 1.2 \times 700$	20	0.29
A-N-T2	$140 \times 3.0 \times 700$	0	0
E-N-T2	$140 \times 3.0 \times 700$	20	0.29

Table 2. Mix proportion of the concrete (unit: kg/m^3).

Water	Cement	Fine Aggregate	Coarse Aggregate	Fly Ash	Superplasticizer (wt.%)
199.0	401.5	836.5	768.5	122.1	0.4

In order to evenly load the columns, the column ends were welded to square steel plates with a thickness and width of 20 and 180 mm, respectively. Once the bottom of the steel tube was welded to a steel plate, concrete was cast into the steel tube. The tube and bottom steel plate acted as molds, and no external vibration was needed. After concrete casting, the samples cured in the experimental room for 28 d. Another steel plate was welded on the top end of the tube before the test. Concrete specimens with dimensions of 150 mm × 150 mm × 150 mm and 150 mm × 150 mm × 300 mm were fabricated with the steel tube columns to measure the concrete strength and modulus of elasticity of the concrete, respectively. Figure 1 displays the major fabrication process of the columns.

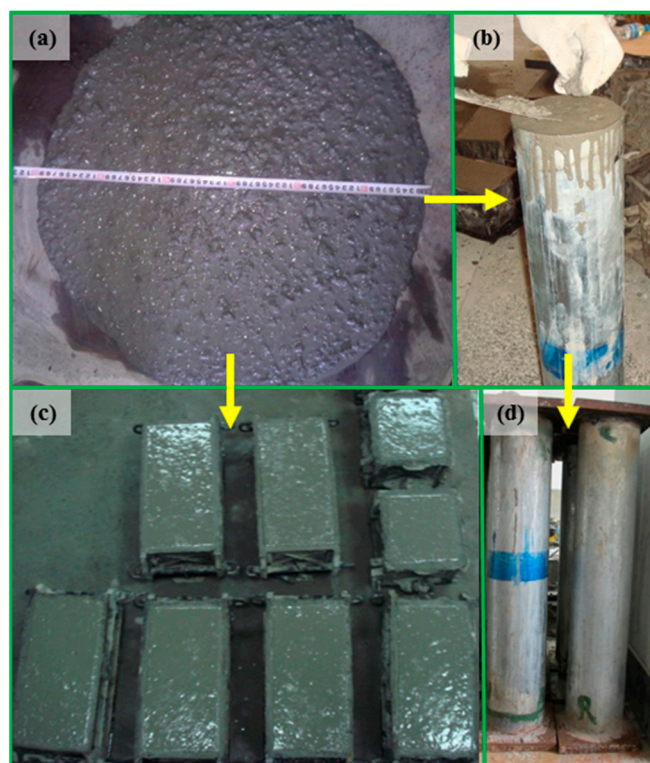


Figure 1. Major fabrication process. (a) The concrete. (b) Casting concrete into steel tube. (c) Concrete specimens. (d) Prepared samples.

2.2. Performance of Materials

Table 3 presents the mechanical properties of the steel tubes, which were measured according to the specification in [47]. The mechanical performance of the concrete was tested according to the specification in [48]. Concrete specimens were prepared with the columns, which were cured under the same conditions as the columns for 28 d. The concrete's modulus of elasticity was 25.7 GPa and its prism strength was 54.4 MP.

Table 3. Mechanical performance of the steel tubes.

Wall Thickness (mm)	Yield Strength (MPa)	Modulus of Elasticity (GPa)	Poisson's Ratio
1.2	345.0	181.0	0.30
3.0	358.3	202.0	0.28

2.3. Test Setup and Procedure

The compressive testing of the columns was conducted using a universal testing machine after 28 d. Figure 2 shows the loading arrangements and schematic. As shown in Figure 2, an eccentric load was applied to the endplate of the columns with a spherical hinge and load-bearing plate, while the load in the axial direction was directly exerted on

the endplate. A steel cylinder with diameter and length of 100 and 180 mm, respectively, was used as the spherical hinge. The load-bearing plate was a cuboid steel plate, and its square width and thickness was 180 and 30 mm, respectively. Strains were measured with a DH3820N strain indicator, which was supplied by Donghua testing technology Co., Ltd. (Taizhou, China). The strain gauges were numbered 1 to 8. Strain gauges 1~4 and 5~8 were used to measure transverse and axial strains, respectively. The average value of the four strains was calculated as the strains along the axial and transverse directions, respectively. Two displacement meters were arranged vertically at the bottom, numbered as 4 and 5, to test the vertical displacements. The lateral deflections were measured using another three displacement meters, numbered as 1 to 3, which were located at the middle height on the left side of the columns.

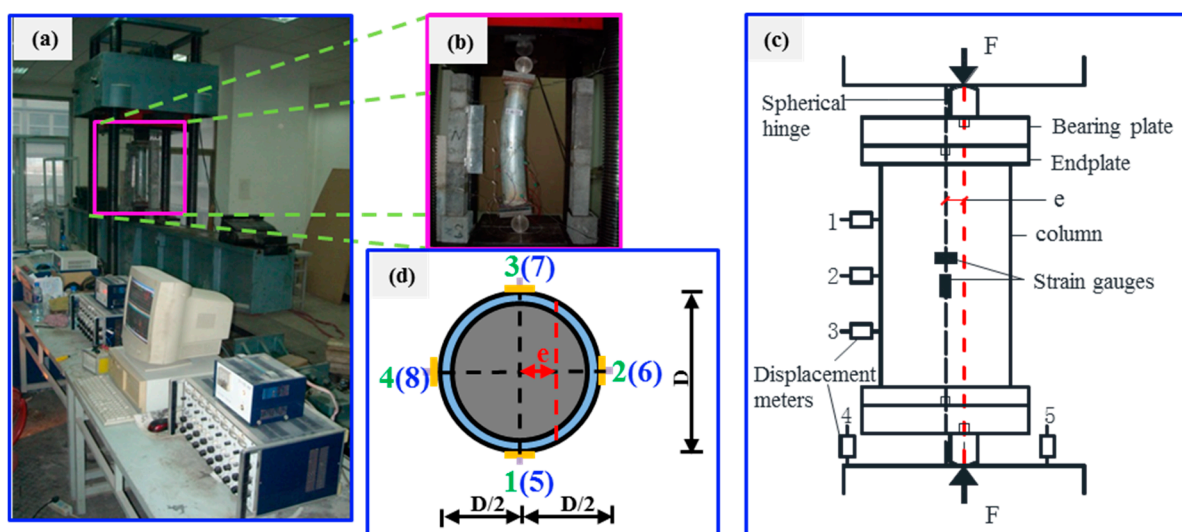


Figure 2. Loading arrangements and schematic. (a) Loading devices. (b) Column under eccentric compression. (c) Schematic of loading devices. (d) Numbers of strain gauges.

Before the formal experiment, a preliminary loading with loading rate set to 0.5 kN/min and loading amplitude of 15 kN was conducted to ensure uniform loading. At the formal experimental stage, loading rate was set to 0.5 mm/min. Loads were continuously exerted on the columns, and the test was stopped when preload fell to 60% of the ultimate capacity. Loading interval was defined as one-fifteenth of the theoretical ultimate capacity. Each of the loading intervals lasted for 3 min. Total testing time of one column was 2 h. Experimental data including displacements, strains, and loads during the test process were collected by an automatic acquisition system.

3. Results and Discussion

3.1. Failure Morphology

The failure morphology of the samples is presented in Figure 3. The eccentric-loaded columns showed obvious buckling and lateral deflection, which is evident in Figure 3. However, the characteristics of the failure modes of the CFST columns under an eccentric load included bending and buckling [38]. Moreover, columns undergoing axial compression displayed evident local bulking and rupture of the steel tube. When wall thickness varied from 1.2 mm to 3.0 mm, the numbers of the bulking are reduced and its locations are transferred from the ends to the middle position. Similarly, the buckling and lateral deflection is also transferred from the end to the middle position. Figure 4 presents the relationship between the load and deformation. The load varies with displacement which is displayed in Figure 4a. It firstly increases gradually to the peak value and then the descend phase decreases rapidly when the columns undergo axial compression, but decrease gently when the columns undergo eccentric compression. Therefore, compared

with columns subjected to an axial compressive load, columns under eccentric compression display better ductility. The curves present a similar development trend under axial or eccentric compression with different wall thicknesses. Nevertheless, the ultimate capacity is increased with increasing wall thickness. The load–longitudinal strain curves were derived from the relationship between the load and the average strain along the axial direction of 5 to 8; as shown in Figure 4b, the strain almost proximately increases linearly with the load until about 75 percent of the peak load. Then, the load varies nonlinearly with the strain. All the load–strain curves present a similar variation trend. However, the axial strains increase faster than the transverse strains. Figure 4c displays load–lateral deflection curves of columns undergoing eccentric compression, which demonstrate that the relationship between the load and lateral deflection has a similar development tendency. Lateral deflections increase slowly before the peak load and then decrease slowly during the whole eccentric loading process.



Figure 3. The columns' failure modes.

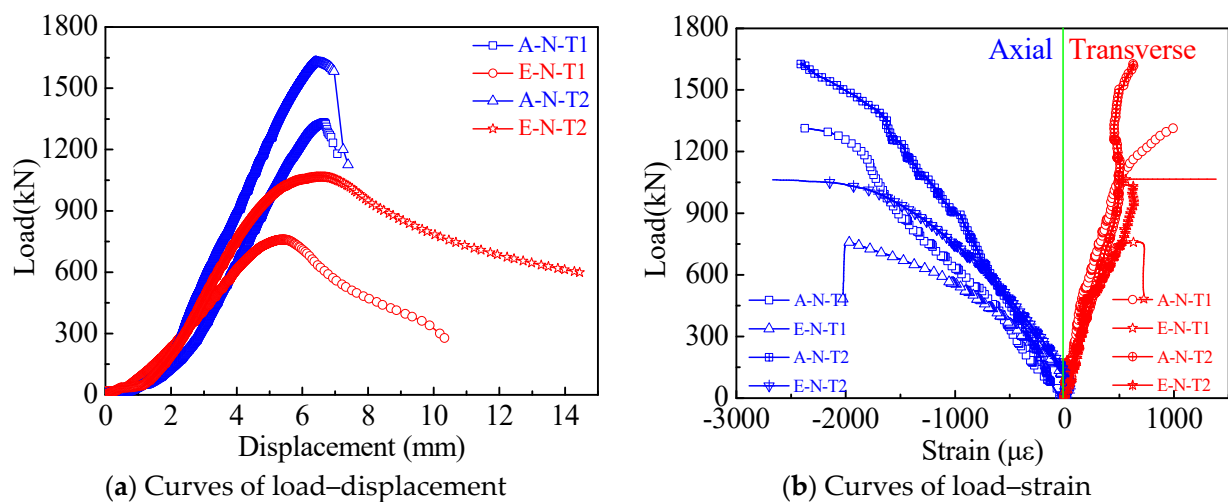


Figure 4. Cont.

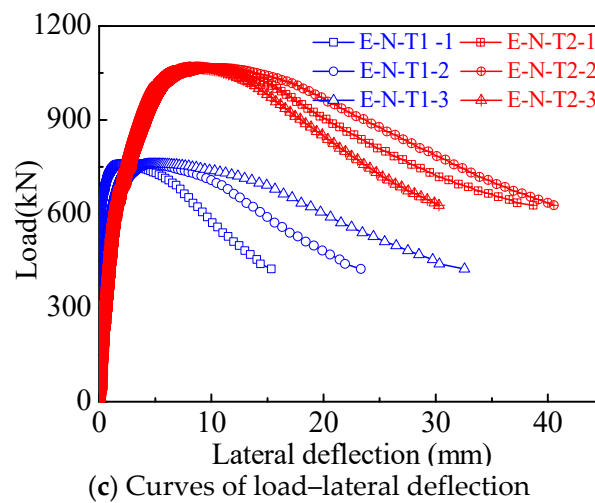


Figure 4. Relationships between deformation and load.

3.2. Theory Calculation Formulas for Ultimate Capacity of Design Codes

To explore the feasibility of predicting the columns' ultimate capacity using the design codes, calculation formulas for the ultimate capacity of six design codes including JCJ 01-89 [49], CECS 28 [50], DL/T 5085 [51], DBJ 13-51-2003 [52], AISC-LRFD-1999 [53], and BS 5400 [54] are summarized as follows. The prediction of the ultimate capacity was calculated using these codes; after that, a comparison between these values and the experimental results was conducted.

The calculation formula for the ultimate capacity of the code JCJ 01-89 [49] is expressed as Equation (1):

$$N = \gamma \varphi_e (A_s f_s + K_1 A_c f_c) \quad (1)$$

where K_1 is the increase coefficient of the concrete strength, f_s represents the steel tube's design compressive strength, f_c is the concrete's design compressive strength, A_s stands for the steel tube's cross-sectional area, A_c is the cross-sectional area of the concrete, φ_e is the reduction coefficient of eccentric compression, and γ is the correction of φ_e .

The formula for the ultimate capacity of the code CECS 28:90 [50] is expressed as Equation (2):

$$N = \varphi_1 \varphi_e A_c f_c (1 + \sqrt{\theta} + \theta) \quad (2)$$

where φ_1 is the reduction coefficient of the slenderness ratio.

The ultimate capacity of the code DL/T 5085-1999 [51] is calculated using Equations (3)–(13). If $N/A_{sc} \geq 0.2\varphi f_{sc}$,

$$\frac{N}{\varphi A_{sc} f_{sc}} + \frac{\beta_m M}{1.071(1 - 0.4N/N_E)\gamma_m W_{sc} f_{sc}} \leq 1 \quad (3)$$

If $N/A_{sc} < 0.2\varphi f_{sc}$,

$$\frac{N}{1.4\varphi A_{sc} f_{sc}} + \frac{\beta_m M}{(1 - 0.4N/N_E)\gamma_m W_{sc} f_{sc}} \leq 1 \quad (4)$$

where β_m represents the moment coefficient, and its value is in accordance with code GB 50017-2003 [55], and γ_m is the flexural plasticity development coefficient of the component in the sectional area: if $\xi \geq 0.85$, $\gamma_m = 1.4$; otherwise, $\gamma_m = 1.2$. The standard confinement coefficient ξ is calculated by Equation (5):

$$\xi = A_s f_y / (A_c f_{ck}) \quad (5)$$

where f_y is the steel tube yield strength.

f_{sc} stands for the composite design compressive strength, and it is calculated using Equation (6):

$$f_{sc} = (1.212 + B_1\zeta_0 + C_1\zeta_0^2)f_c \quad (6)$$

where B_1 and C_1 are coefficients, which are determined as

$$B_1 = 0.1759 f_y / 235 + 0.974 \quad (7)$$

$$C_1 = -0.1038 f_{ck} / 20 + 0.0309 \quad (8)$$

where ζ_0 is the design confinement coefficient, which can be calculated using Equation (9):

$$\zeta_0 = A_s f / (A_c f_c) \quad (9)$$

where N_E represents the Euler critical load, which is determined by Equation (10):

$$N_E = \pi^2 E_{sc} A_{sc} / \lambda^2 \quad (10)$$

where A_{sc} stands for the total sectional area, and E_{sc} is the composite modulus of elasticity and is computed using Equation (11):

$$E_{sc} = f_{scp} / \varepsilon_{scp} \quad (11)$$

where f_{scp} is the proportional limit, and ε_{scp} is the strain under the proportional limit. They can be calculated using Equations (12) and (13), respectively:

$$f_{scp} = [0.192(f_y / 235) + 0.488] f_{scy} \quad (12)$$

$$\varepsilon_{scp} = 3.25 \times 10^{-6} f_y \quad (13)$$

where f_{scy} is the standard composite axial strength.

The ultimate capacity of the code DBJ 13-51-2003 [52] is calculated using Equations (14)–(21). If $N / (A_{sc} f_{sc}) \geq 2\varphi^3 \eta_0$,

$$\frac{N}{A_{sc} f_{sc}} + \left(\frac{a}{d}\right) \frac{\beta_m M}{\gamma_m W_{sc} f_{sc}} \leq 1 \quad (14)$$

If $N / (A_{sc} f_{sc}) < 2\varphi^3 \eta_0$,

$$\frac{-bN^2}{(A_{sc} f_{sc})^2} - \frac{cN}{A_{sc} f_{sc}} + \left(\frac{1}{d}\right) \frac{\beta_m M}{\gamma_m W_{sc} f_{sc}} \leq 1 \quad (15)$$

where φ is the stability coefficient, and γ_m is a coefficient, which can be calculated using Equation (16):

$$\gamma_m = 1.1 + 0.48 \ln(\zeta + 0.1) \quad (16)$$

W_{sc} is the flexural modulus of the sectional area; for the circular steel tube, it can be calculated using Equation (17):

$$W_{sc} = \pi D^3 / 32 \quad (17)$$

where D represents the steel tube's diameter.

a , b , c , and d are coefficients; they are calculated using Equations (18)–(21):

$$a = 1 - 2\varphi^2 \eta_0 \quad (18)$$

$$b = \frac{1 - \zeta_0}{\varphi^3 \eta_0^2} \quad (19)$$

$$c = \frac{2(\zeta_0 - 1)}{\eta_0} \quad (20)$$

$$d = 1 - 0.4 \left(\frac{N}{N_E} \right) \quad (21)$$

The ultimate capacity of the code AISC-LRFD-1999 [53] is calculated using the following equations. If $\left(\frac{N}{\phi_c N_u} \geq 0.2 \right)$,

$$\frac{N}{\phi_c N_u} + \frac{8M}{9\phi_b M_u} \leq 1 \quad (22)$$

If $\left(\frac{N}{\phi_c N_u} < 0.2 \right)$,

$$\frac{N}{2\phi_c N_u} + \frac{8M}{\phi_b M_u} \leq 1 \quad (23)$$

where N stands for the design axial force, M is the design bending moment, both ϕ_c and ϕ_b are the coefficient, and their values are 0.85 and 0.9, respectively. N_u stands for the axial ultimate load, and it can be calculated using Equation (24):

$$N_u = F_{cr} A_s \quad (24)$$

where F_{cr} is the critical force; it can be computed as follows:

$$F_{cr} = \left(0.658^{\lambda_c^2} \right) F_{my} \quad (\lambda_c \leq 1.5) \quad (25)$$

$$F_{cr} = \left(0.877 / \lambda_c^2 \right) F_{my} \quad (\lambda_c > 1.5) \quad (26)$$

where λ_c represents the slenderness ratio; it is expressed as

$$\lambda_c = \frac{kL}{r\pi} \sqrt{\frac{F_{my}}{E_m}} \quad (27)$$

where k stands for the effective length coefficient, r stands for the gyration radius, and F_{my} is the equivalent yield strength, which is expressed as Equation (28):

$$F_{my} = f_y + 0.85 f_c' \left(\frac{A_c}{A_s} \right) \quad (28)$$

E_m represents the equivalent modulus of elasticity, which is expressed as Equation (29):

$$E_m = E_s + 0.4 E_c \left(\frac{A_c}{A_s} \right) \quad (29)$$

where E_s represents the steel tube's modulus of elasticity, and E_c is the concrete's modulus of elasticity.

M_u is the flexural capacity, which is determined using Equation (30):

$$M_u = Z f_y \quad (30)$$

where Z is the plastic bending modulus, which can be calculated as follows:

$$Z = \left[D^3 - (D - 2t)^3 \right] / 6 \quad (31)$$

The ultimate capacity formulas of the code BS 5400 [54] are expressed as follows:

$$N \leq N_u \left[k_1 - (k_1 - k_2 - 4k_3) \frac{M}{M_u} - 4k_3 \left(\frac{M}{M_u} \right)^2 \right] \quad (32)$$

where N stands for the design axial force, and M is the bending moment. N_u is the ultimate bearing capacity under axial load, which can be calculated as follows:

$$N_u = A_s f_{yr} / \gamma_s + 0.675 A_c f_{cc} / \gamma_c \quad (33)$$

where γ_s and γ_c represent partial coefficients of steel and concrete, respectively; their values are 1.1 and 1.5, respectively. f_{yr} stands for steel yield strength after reduction, which can be calculated as follows:

$$f_{yr} = C_2 f_y \quad (34)$$

$$C_2 = 0.76 + 0.0096(L/D) \quad (35)$$

f_{cc} is the concrete strength when subjected to triaxial compression, which is expressed as Equation (36):

$$f_{cc} = f_{cu} + f_y C_1 \frac{t}{D} \quad (36)$$

$$C_1 = 0.0129(L/D)^2 - 0.7055(L/D) + 9.5275 \quad (37)$$

M_u is the flexural capacity and is expressed as follows:

$$M_u = S \frac{f_y}{\gamma_s} (1 + 0.01m) \quad (38)$$

$$S = t^3 \left(\frac{D}{t} - 1 \right)^2 \quad (39)$$

k_1 is the stability coefficient, which can be calculated as follows:

$$k_1 = 1 \quad \lambda < 0.2 \quad (40)$$

$$k_1 = \frac{A - \sqrt{A^2 - 4\lambda^2}}{2\lambda^2} \quad \lambda \geq 0.2 \quad (41)$$

$$A = 1 + 0.158\sqrt{\lambda^2 - 0.04} + \lambda^2 \quad (42)$$

$$\lambda = L/l_e \quad (43)$$

$$l_e = \pi \sqrt{\frac{E_s I_s + E_c I_c}{N_u}} \quad (44)$$

where E_s and E_c are the modulus of elasticity of steel and concrete, respectively. I_s and I_c stand for the inertia moment of the steel tube and concrete, respectively. k_2 and k_3 can be calculated as follows:

$$k_2 = k_{20} \times [115 - 30 \times (1.8 - \alpha_c) - 100\lambda] / 55 \quad (0 \leq k_2 \leq k_{20}) \quad (45)$$

$$k_{20} = 0.9\alpha_c^2 + 0.2 \quad (0 \leq k_{20} \leq 0.75) \quad (46)$$

$$k_3 = k_{30} + \frac{[0.9 \times (\alpha_c^2 - 0.5) + 0.15] \lambda}{1 + \lambda^3} \quad (k_3 \geq 0) \quad (47)$$

$$k_{30} = 0.04 - \frac{\alpha_c}{15} \quad (k_{30} \geq 0) \quad (48)$$

$$\alpha_c = \frac{0.45 f_{cc} A_c}{N_u} \quad (0.1 < \alpha_c < 0.8) \quad (49)$$

Pacheco et al. suggest that the conversion coefficient of 150 mm cubic to cylinder with a diameter of 150 mm for recycled concrete is 0.77 [56]. Additionally, the conversion coefficient of 150 mm cubic to prism with dimensions of 150 mm × 150 mm × 300 mm for recycled concrete is 0.67 [57,58].

3.3. Comparison of the Ultimate Load

The ultimate capacities of the columns undergoing eccentric and axial compression from calculated results using different design codes and experimental results are represented by N_{uc} and N_{ue} , respectively, in Table 4. Table 5 compares N_{uc} and N_{ue} . Table 6 shows the statistical characteristics of the comparison results. A comparison of the ultimate capacities from the experimental results and calculated results using different specifications is displayed in Figure 5.

Table 4. Ultimate capacities from calculated results and experimental values.

Numbers	N_{ue} (kN)	N_{uc} (kN)					
		JCJ	CECS	DL/T	DBJ	AISC	BS
A-N-T1	1331.0	1117.0	1047.8	1059.9	899.4	813.5	809.5
E-N-T1	759.0	711.3	679.6	555.3	593.4	267.3	569.7
A-N-T2	1627.8	1582.4	1426.0	1356.7	1187.0	1028.3	1181.0
E-N-T2	1065.8	978.6	918.7	713.1	465.0	512.5	877.0

Table 5. Comparison between the ultimate capacities of the experimental results and calculated results.

Numbers	N_{uc}/N_{ue}					
	JCJ	CECS	DL/T	DBJ	AISC	BS
A-N-T1	0.84	0.79	0.80	0.68	0.61	0.61
E-N-T1	0.94	0.90	0.73	0.78	0.35	0.75
A-N-T2	0.97	0.88	0.83	0.73	0.63	0.73
E-N-T2	0.92	0.86	0.67	0.44	0.48	0.82

Table 6. Statistical properties of the comparison between the ultimate capacities of the experimental results and calculated values.

Numbers	Parameters	N_{uc}/N_{ue}					
		JCJ	CECS	DL/T	DBJ	AISC	BS
Axial-loaded	Average value	0.91	0.83	0.81	0.70	0.62	0.67
	Variation coefficient	0.09	0.06	0.03	0.04	0.02	0.08
Eccentric-loaded	Average value	0.93	0.88	0.70	0.61	0.42	0.79
	Variation coefficient	0.01	0.02	0.04	0.24	0.09	0.05
Eccentric-loaded average value to axial-loaded average value		1.02	1.06	0.86	0.87	0.67	1.18

It can be seen from Table 4 that the experimental ultimate capacities of A-N-T1, A-N-T2, E-N-T1, and E-N-T2 are 1331.0, 1627.8, 759.0, and 1065.8 kN, respectively. Moreover, the ranges of the calculated ultimate capacities of A-N-T1, A-N-T2, E-N-T1, and E-N-T2 using different design codes are 809.5 kN~1117.0 kN, 1028.3 kN~1582.4 kN, 267.3 kN~711.3 kN, and 465.0 kN~978.6 kN, respectively. This clearly demonstrates that the calculated ultimate capacities are correspondingly lower than those of the experimental results.

Table 5 gives the ratio ranges of calculated ultimate capacities to tested results corresponding to A-N-T1, A-N-T2, E-N-T1, and E-N-T2. The ratios range from 0.61 to 0.84, 0.63 to 0.97, 0.35 to 0.94, and 0.44 to 0.92, respectively. This indicates that the calculated ultimate capacity is conservative and safe. Moreover, the calculated ultimate capacities using the codes AISC-LRFD and JCJ 01-89 are the lowest and the highest, respectively. Thus, AISC-LRFD and JCJ 01-89 are the most conservative and the most accurate for the ultimate capacity calculation. Similarly, the ultimate capacity prediction results of the CFST columns were 25% conservative using code AISC-LRFD [8]. The different specifications predicted the ultimate capacity with different precision due to variations in the considered factors, such as the confinement effect of the steel tube on the concrete, the reduction coefficients of materials, and the eccentricity. For example, ACI [59] ignores the contribution of the confinement effect of the steel tube on the concrete, which can improve the ultimate capacity. Additionally, EC4 [60] takes into account the confinement effect, but it provides relatively conservative predictions [61].

Table 6 displays the statistical properties of the comparison between the ultimate capacities of the experimental results and calculated results. The average value and variation coefficient of the ratio of the calculated ultimate capacities to experimental ultimate capacities (N_{uc}/N_{ue}) of A-N-T1 and A-N-T2 are within the range of 0.62~0.91 and 0.02~0.09, respectively. Additionally, the average value and variation coefficient of N_{uc}/N_{ue} of the eccentric compression columns E-N-T1 and E-N-T2 are within the range of 0.42~0.93 and 0.01~0.24, respectively. This implies that the decrease ratio of calculated ultimate capacity to experimental ultimate capacity of the eccentric compression columns is larger than that of the axial compression columns.

The ratios of the average value of N_{uc}/N_{ue} of the columns under eccentric load to the average value of N_{uc}/N_{ue} of the axial-loaded columns are in the range of 0.67~1.18. This indicates that the predicted ultimate capacity of the eccentric compression columns using design codes is smaller than that of the axial compression columns. Figure 5 compares the ultimate capacities of the tested results and the calculated results using different design codes. It indicates that the predicted ultimate capacities are correspondingly smaller than those of the experimental results.

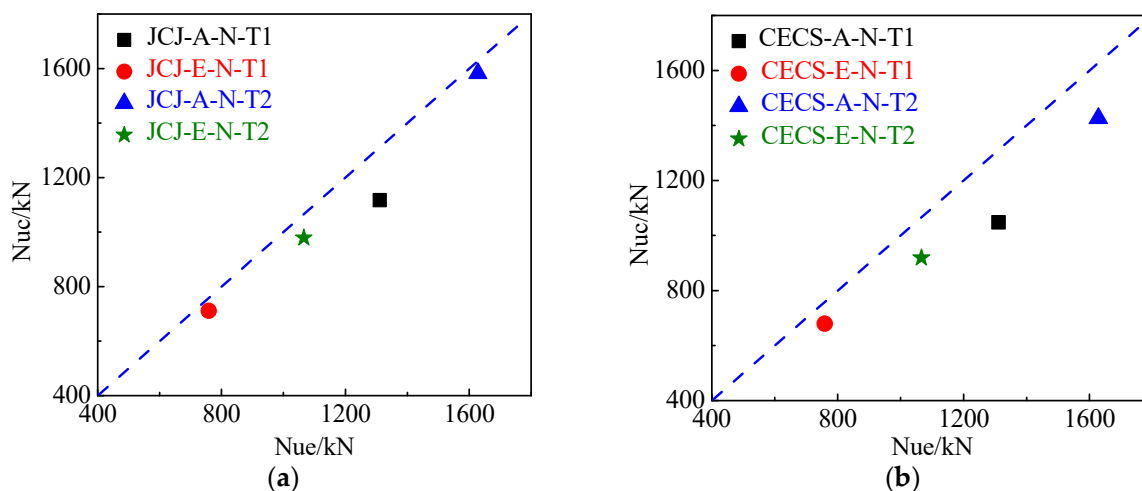


Figure 5. Cont.

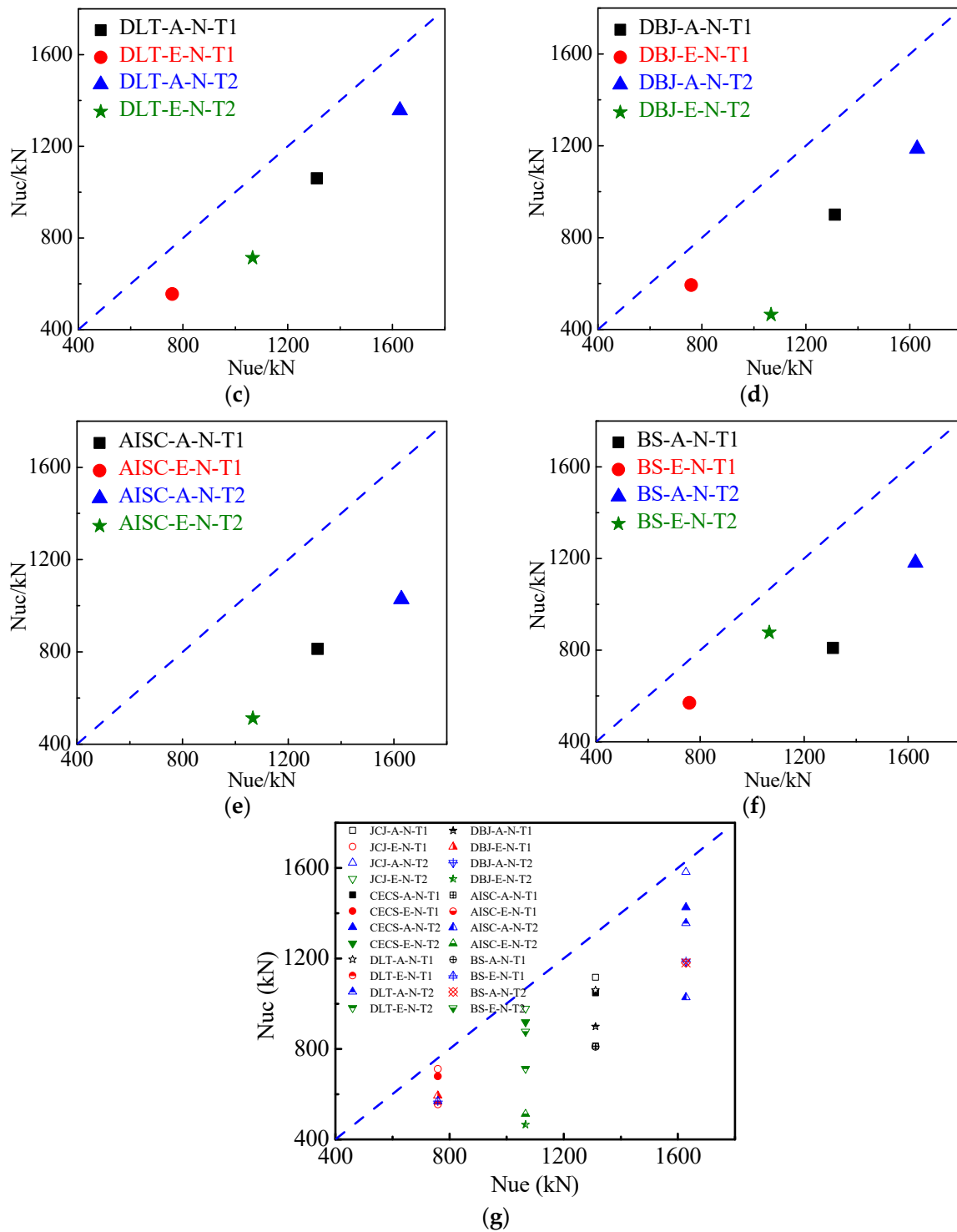


Figure 5. Comparison of the ultimate capacities from experimental results and calculated results. (a) JCI 01–89; (b) CECS 28:90; (c) DL/T 5085–1999; (d) DBJ 13–51–2003; (e) AISC–LRFD; (f) BS 5400; (g) Comparison of the ultimate capacities from experimental results and calculated results using 6 different design codes.

4. Conclusions

In this study, we first fabricated SCFTST columns. Then, the eccentric compression behaviors of the columns were analyzed in depth. Following that, a comparison of the ultimate capacities from experimental results and computed results using different specifications was conducted sequentially. Moreover, the influence of eccentric ratios of the

load and wall thickness on the eccentric compression behaviors have been discussed. The conclusions drawn from the results are as follows:

- (1) The columns undergoing eccentric compression displayed major failure modes of buckling and lateral deflection, while the axial compression columns displayed buckling and rupture. In addition, the buckling and lateral deflection was transferred from the bottom to middle location when the wall thickness was increased.
- (2) The ultimate capacity increased with increasing wall thickness. With loading continuing after the peak load, the load decreased gently with increasing lateral deflection. However, the load decreased rapidly with increasing displacement.
- (3) The calculated ultimate capacities were correspondingly lower than the experimental values. The percentages of the calculated maximum capacities to experimental results of the columns under eccentric compression were within the range of 0.35 to 0.94, while those of the columns under axial compression were within the range of 0.61 to 0.97. This indicates that the calculated ultimate capacity is conservative and safe. The codes AISC-LRFD and JCJ 01-89 achieved the most conservative and the most precise results, respectively, when predicting the ultimate capacity.
- (4) The average value of the ratio of the calculated ultimate capacity to the experimental ultimate capacity of the eccentric compression columns was within the range of 0.42~0.93, while that of the columns under axial compression was within the range of 0.62~0.91.

These results imply that the SCFTST columns have huge potential for application in the civil industry. However, few studies have concentrated on columns subjected to eccentric compression with different parameters, and a limitation of our study is the small number of specimens; therefore, more research is needed. For example, the effect of slenderness, eccentricity, section type, and the strength of materials on the eccentric loading behaviors of the columns requires more investigation. The deviations of the ultimate capacity prediction of each code lack an in-depth physical explanation. Finite element analysis of the performance of these columns also needs to be conducted. Moreover, for the columns to be applied in large-scale structural components, investigations on their structural performance, including bending and shear behavior, are worthwhile.

Author Contributions: Conceptualization, Y.J.; methodology, Y.W.; formal analysis, Y.W.; investigation, Y.W.; resources, S.S. and L.Z.; data curation, Y.W.; writing—original draft preparation, Y.W.; writing—review and editing, Y.W., S.S. and L.Z.; supervision, Y.J.; project administration, Y.J.; funding acquisition, S.S. and L.Z. All authors have read and agreed to the published version of the manuscript.

Funding: This research was funded by The Young backbone teachers of ordinary universities in Hunan Province of 2023, grant number [2023], No. 318, documents issued by the Education Department of Hunan Province; The Project of China Construction Engineering Co., Ltd., grant number CSCEC-2021-Q-56; The Project of China Construction Second Engineering Bureau Co., Ltd., grant number 2021ZX000004; The National Science Foundation of China, grant number 52368031; The China Postdoctoral Science Foundation, grant number 2022M713497; The Jiangxi Provincial Natural Science Foundation, grant number 20224BAB204067; The Jiangxi Provincial Department of Transportation Science and Technology Project, grant number 2022H0017; and the APC was funded by Hunan University of Arts and Science.

Data Availability Statement: Data are contained within the article.

Acknowledgments: The authors express their appreciation to Yongjun Chen.

Conflicts of Interest: Shengwei Sun is employed by the China Construction Second Engineering Bureau Co., Ltd. The remaining authors declare no conflict of interest.

References

1. Zheng, J.; Wang, J. Concrete-filled steel tube arch bridges in China. *Engineering* **2018**, *4*, 143–155. [[CrossRef](#)]
2. Xie, K.; Wang, H.; Guo, X.; Zhou, J. Study on the safety of the concrete pouring process for the main truss arch structure in a long-span concrete-filled steel tube arch bridge. *Mech. Adv. Mater. Struct.* **2021**, *28*, 731–740. [[CrossRef](#)]

3. Xu, F.; Chen, J.; Jin, W. Experimental investigation of thin-walled concrete-filled steel tube columns with reinforced lattice angle. *Thin-Walled Struct.* **2014**, *84*, 59–67. [[CrossRef](#)]
4. Hassanein, M.F.; Elchalakani, M.; Karrech, A.; Patel, V.I.; Yang, B. *Behaviour of Concrete-Filled Double-Skin Short Columns under Compression through Finite Element Modelling: SHS Outer and SHS Inner Tubes*; Elsevier: Amsterdam, The Netherlands, 2018.
5. Ayough, P.; Sulong, N.R.; Ibrahim, Z. Analysis and review of concrete-filled double skin steel tubes under compression. *Thin-Walled Struct.* **2020**, *148*, 106495. [[CrossRef](#)]
6. Huang, W.P.; Yuan, Q.; Tan, Y.L.; Wang, J.; Liu, G.L.; Qu, G.L.; Li, C. An innovative support technology employing a concrete-filled steel tubular structure for a 1000-m-deep roadway in a high in situ stress field. *Tunn. Undergr. Space Technol.* **2018**, *73*, 26–36. [[CrossRef](#)]
7. Zhang, J.; Liu, L.; Cao, J.; Yan, X.; Zhang, F. Mechanism and application of concrete-filled steel tubular support in deep and high stress roadway. *Constr. Build. Mater.* **2018**, *186*, 233–246. [[CrossRef](#)]
8. Liu, D. Behaviour of high strength rectangular concrete-filled steel hollow section columns under eccentric loading. *Thin-Walled Struct.* **2004**, *42*, 1631–1644. [[CrossRef](#)]
9. Xiong, M.; Xiong, D.; Liew, J.R. Axial performance of short concrete filled steel tubes with high-and ultra-high-strength materials. *Eng. Struct.* **2017**, *136*, 494–510. [[CrossRef](#)]
10. De Oliveira, W.L.A.; De Nardin, S.; de Cresce El, A.L.H.; El Debs, M.K. Influence of concrete strength and length/diameter on the axial capacity of CFT columns. *J. Constr. Steel Res.* **2009**, *65*, 2103–2110. [[CrossRef](#)]
11. Gupta, P.K.; Sarda, S.M.; Kumar, M.S. Experimental and computational study of concrete filled steel tubular columns under axial loads. *J. Constr. Steel Res.* **2007**, *63*, 182–193. [[CrossRef](#)]
12. Guler, S.; Copur, A.; Aydogan, M. A comparative study on square and circular high strength concrete-filled steel tube columns. *Adv. Steel Constr.* **2014**, *10*, 234–247.
13. Knowles, R.B.; Park, R. Strength of concrete filled steel tubular columns. *J. Struct. Div.* **1969**, *95*, 2565–2588. [[CrossRef](#)]
14. Prion, H.G.; Boehme, J. Beam-column behaviour of steel tubes filled with high strength concrete. *Can. J. Civ. Eng.* **1994**, *21*, 207–218. [[CrossRef](#)]
15. Schneider, S.P. Axially loaded concrete-filled steel tubes. *J. Struct. Eng.* **1998**, *124*, 1125–1138. [[CrossRef](#)]
16. Matsui, C. Slender Concrete Filled Steel Tubular Columns Combined Compressionsnd Bending, Strutural Steel. *Steel-Concert. Compos. Struct.* **1995**, *3*, 29–36.
17. Hu, H.T.; Huang, C.S.; Wu, M.H.; Wu, Y.M. Nonlinear analysis of axially loaded concrete-filled tube columns with confinement effect. *J. Struct. Eng.* **2003**, *129*, 1322–1329. [[CrossRef](#)]
18. Zhu, L.; Ma, L.; Bai, Y.; Li, S.; Song, Q.; Wei, Y.; Zhang, L.; Zhang, Z.; Sha, X. Large diameter concrete-filled high strength steel tubular stub columns under compression. *Thin-Walled Struct.* **2016**, *108*, 12–19. [[CrossRef](#)]
19. Zhou, X.; Mou, T.; Tang, H.; Fan, B. Experimental study on ultrahigh strength concrete filled steel tube short columns under axial load. *Adv. Mater. Sci. Eng.* **2017**, *2017*, 8410895. [[CrossRef](#)]
20. Liao, F.Y.; Hou, C.; Zhang, W.J.; Ren, J. Experimental investigation on sea sand concrete-filled stainless steel tubular stub columns. *J. Constr. Steel Res.* **2019**, *155*, 46–61. [[CrossRef](#)]
21. Xu, L.; Zhou, P.; Chi, Y.; Huang, L.; Ye, J.; Yu, M. Performance of the high-strength self-stressing and self-compacting concrete-filled steel tube columns subjected to the uniaxial compression. *Int. J. Civ. Eng.* **2018**, *16*, 1069–1083. [[CrossRef](#)]
22. Uy, B. Strength of concrete filled steel box columns incorporating local buckling. *J. Struct. Eng.* **2000**, *126*, 341–352. [[CrossRef](#)]
23. Liang, Q.Q.; Uy, B. Parametric study on the structural behaviour of steel plates in concrete-filled fabricated thin-walled box columns. *Adv. Struct. Eng.* **1998**, *2*, 57–71. [[CrossRef](#)]
24. Liang, Q.Q. Strength and ductility of high strength concrete-filled steel tubular beam-columns. *J. Constr. Steel Res.* **2009**, *65*, 687–698. [[CrossRef](#)]
25. Liang, Q.Q.; Uy, B.; Liew, J.R. Nonlinear analysis of concrete-filled thin-walled steel box columns with local buckling effects. *J. Constr. Steel Res.* **2006**, *62*, 581–591. [[CrossRef](#)]
26. Zhang, Y.; Xu, C.; Lu, X. Experimental study of hysteretic behaviour for concrete-filled square thin-walled steel tubular columns. *J. Constr. Steel Res.* **2007**, *63*, 317–325. [[CrossRef](#)]
27. Goto, Y.; Jiang, K.; Obata, M. Stability and ductility of thin-walled circular steel columns under cyclic bidirectional loading. *J. Struct. Eng.* **2006**, *132*, 1621–1631. [[CrossRef](#)]
28. Gajalakshmi, P.; Helena, H.J. Behaviour of concrete-filled steel columns subjected to lateral cyclic loading. *J. Constr. Steel Res.* **2012**, *75*, 55–63. [[CrossRef](#)]
29. Wang, Y.; Xiao, L.; Jiang, C.; Jia, Y.; Yang, G.; Li, M.; Tang, X.; Chen, D. Axial loading behaviour of self-compacting concrete-filled thin-walled steel tubular stub columns. *Adv. Civ. Eng.* **2021**, *2021*, 8861340. [[CrossRef](#)]
30. Wu, B.; Lin, L.; Zhao, J.; Shen, C. Compressive behaviour of thin-walled square tubular columns filled with high-strength steel section and precast compound concrete segments. *Thin-Walled Struct.* **2020**, *151*, 106710. [[CrossRef](#)]
31. Lim, J.; Eom, T. Compression tests of octagonal concrete-filled thin-walled tube columns. *Eng. Struct.* **2020**, *221*, 111082. [[CrossRef](#)]
32. Dey, S.; Kumar, V.P.; Goud, K.R.; Basha, S.K.J. State of art review on self compacting concrete using mineral admixtures. *J. Build. Pathol. Rehabil.* **2021**, *6*, 18. [[CrossRef](#)]
33. Faraj, R.H.; Mohammed, A.A.; Omer, K.M. Self-compacting concrete composites modified with nanoparticles: A comprehensive review, analysis and modeling. *J. Build. Eng.* **2022**, *50*, 104170. [[CrossRef](#)]

34. Fiol, F.; Revilla-Cuesta, V.; Thomas, C.; Manso, J.M. Self-compacting concrete containing coarse recycled precast-concrete aggregate and its durability in marine-environment-related tests. *Constr. Build. Mater.* **2023**, *377*, 131084. [[CrossRef](#)]
35. GB 50936-2014; Technical Code for Concrete Filled Steel Tubular Structures. Architecture Industrial Press of China: Beijing, China, 2014.
36. Zhang, F.; Xia, J.; Li, G.; Guo, Z.; Chang, H.; Wang, K. Degradation of axial ultimate load-bearing capacity of circular thin-walled concrete-filled steel tubular stub columns after corrosion. *Materials* **2020**, *13*, 795. [[CrossRef](#)]
37. Wu, B.; Lin, L.; Zhao, J.; Yan, H. Creep behavior of thin-walled circular steel tubular columns filled with demolished concrete lumps and fresh concrete. *Constr. Build. Mater.* **2018**, *187*, 773–790. [[CrossRef](#)]
38. Yu, F.; Qin, C.; Wang, S.; Jiang, J.; Fang, Y. Stress-strain relationship of recycled self-compacting concrete filled steel tubular column subjected to eccentric compression. *Front. Struct. Civ. Eng.* **2020**, *14*, 760–772. [[CrossRef](#)]
39. Wang, Y.; Zhang, L.; Jia, Y.; Li, L. Experimental Study on Self-Compacting Concrete-Filled Thin-Walled Steel Tube Columns. *Buildings* **2022**, *12*, 2134. [[CrossRef](#)]
40. Chen, J.; Jin, W. Experimental investigation of thin-walled complex section concrete-filled steel stub columns. *Thin-Walled Struct.* **2010**, *48*, 718–724. [[CrossRef](#)]
41. Jiang, A.; Chen, J.; Jin, W. Experimental investigation and design of thin-walled concrete-filled steel tubes subject to bending. *Thin-Walled Struct.* **2013**, *63*, 44–50. [[CrossRef](#)]
42. Han, L.; Li, W.; Bjorhovde, R. Developments and advanced applications of concrete-filled steel tubular (CFST) structures: Members. *J. Constr. Steel Res.* **2014**, *100*, 211–228. [[CrossRef](#)]
43. Yu, Z.; Ding, F.; Cai, C.S. Experimental behavior of circular concrete-filled steel tube stub columns. *J. Constr. Steel Res.* **2007**, *63*, 165–174. [[CrossRef](#)]
44. Wang, Y.; Chen, J.; Geng, Y. Testing and analysis of axially loaded normal-strength recycled aggregate concrete filled steel tubular stub columns. *Eng. Struct.* **2015**, *86*, 192–212. [[CrossRef](#)]
45. Tran, V.; Thai, D.; Nguyen, D. Practical artificial neural network tool for predicting the axial compression capacity of circular concrete-filled steel tube columns with ultra-high-strength concrete. *Thin-Walled Struct.* **2020**, *151*, 106720. [[CrossRef](#)]
46. JCJ/T 283-2012; Technical Specification for Application of Self-Compacting Concrete. China Architecture & Building Press: Beijing, China, 2012.
47. GB/T 228.1-2021; Standard for Tensile Testing Method of Metallic Materials. Standards Press of China: Beijing, China, 2021.
48. GB/T 50081-2002; Standard for Test Methods for Mechanical Properties of Ordinary Concrete. China Construction Industry Press: Beijing, China, 2002.
49. JCJ 01-89; Design and Construction Specification for Concrete-Filled Steel Tubular Structures. Tongji University Press: Shanghai, China, 1989.
50. CECS 28: 90; Technical Specification for Concrete-Filled Steel Tubular Structures. China Planning Press: Beijing, China, 1991.
51. DL/T 5085-1999; Code for Design of Steel-Concrete Composite Structure. China Electric Power Press: Beijing, China, 1999.
52. DBJ 13-51-2003; Technical Specification for Concrete-Filled Steel Tubular Structures. Fujian Engineering Construction Science and Technology Standardization Association: Fuzhou, China, 2003.
53. AISC-LRFD-1999; Load and Resistance factor Design Specification for Structural Steel Buildings. American Institute of Steel Construction: Chicago, IL, USA, 1999.
54. BS 5400 1979; Steel Concrete and Composite Bridges, Part 5: Code of Practice for Design Composite Bridges. British Standards Institution: British, UK, 1979.
55. GB 50017-2003; Code for Design of Steel Structures. China Planning Press: Beijing, China, 2003.
56. Pacheco, J.N.; De Brito, J.; Chastre, C.; Evangelista, L. Probabilistic conversion of the compressive strength of cubes to cylinders of natural and recycled aggregate concrete specimens. *Materials* **2019**, *12*, 280. [[CrossRef](#)] [[PubMed](#)]
57. Lyu, W.; Han, L.; Hou, C. Axial compressive behaviour and design calculations on recycled aggregate concrete-filled steel tubular (RAC-FST) stub columns. *Eng. Struct.* **2021**, *241*, 112452. [[CrossRef](#)]
58. Xiao, J.Z. *Recycled Concrete*; China Architecture & Building Press: Beijing, China, 2008.
59. ACI 318-1999; Building Code Requirements for Structural Concrete and Commentary. Institut A C: Farmington Hills, MI, USA, 1999.
60. EC4-2004; Design of Composite Steel and Concrete Structures. European Committee for Standardization: Brussels, Belgium, 2004.
61. Al-Ani, Y.R. Finite element study to address the axial capacity of the circular concrete-filled steel tubular stub columns. *Thin-Walled Struct.* **2018**, *126*, 2–15. [[CrossRef](#)]

Disclaimer/Publisher’s Note: The statements, opinions and data contained in all publications are solely those of the individual author(s) and contributor(s) and not of MDPI and/or the editor(s). MDPI and/or the editor(s) disclaim responsibility for any injury to people or property resulting from any ideas, methods, instructions or products referred to in the content.